Journal of Cleaner Production xxx (xxxx) 133775

Contents lists available at ScienceDirect

Journal of Cleaner Production

journal homepage: www.elsevier.com/locate/jclepro

Hydrothermal carbonisation of paper sludge: Effect of process conditions on hydrochar fuel characteristics and energy recycling efficiency

Englatina I.N.C. Assis *, Brian Gidudu, Evans M.N. Chirwa

Department of Chemical Engineering, Water Utilisation and Environmental Engineering Division, University of Pretoria, Pretoria, 0002, South Africa

ARTICLE INFO

Handling Editor: Prof. Jiri Jaromir Klemeš

Keywords:
Paper sludge
Hydrothermal carbonisation
Hydrochar
Clean solid fuel
Response surface methodology

ABSTRACT

Current management of solid waste from pulp and paper activities represents an environmental and economic burden worldwide due to pollution emissions. This study investigates the potential of hydrothermal carbonisation (HTC) treatment as a sustainable alternative for producing cleaner and energy-dense solid fuel from paper mill sludge. The effect of process parameters (temperature, reaction time and solid load) on hydrochar fuel formation from paper sludge was evaluated and, for the first time, the paper sludge-derived hydrochar was optimised to maximise the mass yield and calorific value using response surface methodology (RSM). The physicochemical characteristics, thermal fuel behaviour, energy recycling efficiency and electricity generation potential were assessed by proximate and ultimate analysis, thermogravimetry, bomb calorimeter, scanning electron microscopy and process energy assessment. Results showed that hydrochar fuel formation and properties were mainly influenced by the process temperature and residence time, and governed by dehydration and decarboxylation reactions which reduced the atomic H/C and O/C ratios by 35.5% and 64%, respectively. The produced hydrochars presented low sulphur, nitrogen and ash content with a maximum calorific value (HHV) of 22.9 MJ/kg, equivalent to the HHV of coal for commercial utility in South Africa. The HHV of the hydrochar corresponded to a 49.80% increase over the HHV of the initial feedstock. The optimum operating conditions were 231 ± 1 °C and 1.99 h for a hydrochar yield of 74.4% and calorific value of 18.5 MJ/kg. The energy assessment showed that up to 58.34% of the energy produced by hydrochar fuel combustion may be recycled as heat or power, while the remaining 41.66% of the combustion energy could be utilised to sustain the HTC treatment of paper sludge. The substantial water demand was concluded to be a drawback. Thus, water recirculation and the potential to catalyse the HTC reactions to increase overall process efficiency will constitute a future study to make the process more environmentally friendly for industrial-scale application.

Nomenclature

A	Ash
ANOVA	Analysis of variance
C_{char}	Carbon retained in hydrochar
C_D	Carbon densification
CO_2e	Carbon dioxide equivalent emissions
db	Dry basis
E_C	Electricity generated by coal-fired power plant
$E_{consumed}$	Total energy consumed
E_{cost}	Energy cost
E_D	Energy densification
E_{HC}	Electricity generated from hydrochar
$E_{heating}$	Energy required to heat the oven
E_{htc}	Energy consumed for the duration of the HTC reaction
E_Y	Energy yield
FC	Fixed carbon
GHG	Greenhouse gases
HHV	Higher heating value
HTC	Hydrothermal carbonisation
H_Y	Hydrochar yield
η	Average efficiency of coal-fired power plant
PPMS	Pulp and paper mill sludge
Q_{in}	Input energy
Q_{net}	Net energy
Q_{out}	Output energy
RM	Residual moisture

* Corresponding author.
E-mail address: englatina.assis@tuks.co.za (E.I.N.C. Assis).

https://doi.org/10.1016/j.jclepro.2022.133775
Received 15 February 2022; Received in revised form 18 August 2022; Accepted 20 August 2022
0959-6526/

RSM	Response surface methodology
RF	Raw fibre rejects
$t_{htc\ reaction}$	HTC reaction time
VM	Volatile matter

1. Introduction

With the stringent environmental regulations, rising solid-waste management costs, and continuous waste residues generated from pulp and paper production, the sustainable waste management from these streams represents an economic and environmental problem. In South Africa, over 2 million tonnes of pulp are produced every year (Paper Manufactory Association of South Africa, 2015), leading to the generation of 0.5 million tonnes of solid residues in the form of sludge consisting of moisture, organic and inorganic matter (Boshoff et al., 2016). Common disposal methods involve incineration, landfills or land application (Kaur et al., 2020). These practices deteriorate air quality and threaten public health (Bajpai, 2015). The wastewater streams arising from the paper-making process have high microfibre content. The microfibres do not separate easily during primary sedimentation and are highly resistant to degradation during the biological treatment processes in the secondary activated sludge stages. This results in final effluent with high COD and enormous polluting potential (Cabrera, 2017).

Currently, there is an urgency to diversify the energy basket in South Africa to reduce reliance on coal and mitigate the negative environmental impacts by reducing the carbon footprint in the near future (Department of Energy, 2019). Thus, it is of utmost importance to explore the potential of the underutilised wastes as a renewable energy source through the integration of clean, sustainable and effective technologies for waste valorisation. The pulp and paper mill sludge (PPMS) originates from biomass (Holmberg and Gustavsson, 2007). It is mostly composed of lignocellulose (Kaur et al., 2020) which offers good potential for a sustainable energy resource in form of fuel, heat and electricity production. The use of such readily accessible resource can contribute to the reduction of adverse environmental effects such as the potential emission of GHGs, groundwater pollution, and the reduction of landfill spaces. The utilisation of PPMS as a sustainable resource through balancing the production and utilisation of biomass leads to near-zero GHG emissions since the carbon dioxide produced from the combustion of these sources is absorbed as plant regenerate (Srivastava et al., 2021).

Some of the current ways of recovering energy from lignocellulosic wastes include thermal conversion technologies, namely, pyrolysis, gasification (Libra et al., 2011) and torrefaction (Van der Stelt et al., 2011). Recent advancements have improved the efficiency and quality of these processes, making them more reliable for the urgent switch from fossil fuels to renewable energy. These processes are easily adaptable for producing high-quality gaseous, liquid and solid fuels. However, dry thermochemical conversion methods present some limitations; they commonly involve elevated temperatures and active predrying of the substrates, thereby consuming a considerable amount of energy during processing.

When high-moisture biomass is subjected to these processes, water evaporates prior to reaching the desired reaction temperature. The evaporation requires additional energy consumption, which negatively affects the system's energetic balance, resulting in lower net energy efficiency, thereby affecting the process economy. Dry thermochemical processes are more efficient for feedstocks with relatively low moisture; however, PPMS has considerably high-water content ranging from 37% to 99% (Kaur et al., 2020). If water is to be evaporated, the process becomes energy-intensive and inefficient. Alternatively, hydrothermal processes are investigated due to the ability to produce high-quality fuels and materials with different characteristics than their dry initial substrates at lower temperatures and, more importantly, without the need for pre-drying (Kruse et al., 2013). The hydrothermal carbonisation (HTC) process, in particular, is widely utilised to carbonise organic material. HTC effectively produces significant quantities of char, has excellent rates of carbon recovery, and is applicable for a wide variety of feedstocks (Titirici et al., 2007) including corn stover (Fuertes et al., 2010). The exothermic process (Danso-Boateng et al., 2015), mainly affected by temperature (Wang et al., 2018) and residence time (Kannan et al., 2017), lowers the hydrogen and oxygen content while increasing the carbon compositions through hydrolysis, dehydration, decarboxylation, condensation, polymerisation and aromatisation reactions (Gómez et al., 2020) and occurs in hot-compressed water medium typically at subcritical region (180–260 °C) and autogenous pressure (Wang et al., 2018). Aside from its affordability, water is a non-toxic and non-polluting solvent, which makes it an environmentally friendly medium (Knez et al., 2015). HTC treatment is an energy-efficient process and offers promising potential for the sustainable conversion of paper wastes into high-value lignite-like clean solid fuel commonly known as hydrochar (Spitzer et al., 2018).

The mechanisms of hydrochar formation through HTC are mostly elucidated using pure organic substrates such as cellulose (Saha et al., 2019a), hemicellulose (Kang et al., 2012) and lignin model compounds, including guaiacol (Wahyudiono et al., 2007), catechol (Wahyudiono et al., 2009), eugenol (Besse et al., 2015) and phenolic model compounds such as vanillin (Barbier et al., 2012) and diphenyl ether (Penninger et al., 1999). Complex feedstocks such as lignocellulosic biomass (Güleç et al., 2021), sewage waste (Spitzer et al., 2018), municipal wastewater sludge (Chen et al., 2020), olive wastes (Yay et al., 2021) including from different pollution sources (Volpe et al., 2018) have also been explored to understand the reaction pathways involved. The physicochemical characteristics of the solid product, such as high energetic densities, increased carbon content and improved dewaterability allow hydrochar to be used directly as fuel to generate power (Fang et al., 2018). In addition, various studies have reported hydrochar with decreased levels of inorganic minerals, including Si, K, Na, Cl, P, Ca, Mg and Fe (Smith et al., 2016), which are known to cause toxic emissions, fouling, slagging and corrosion in combustion chambers (Lin et al., 2015).

The majority of the research on the energy potential of hydrochar in previous studies focuses on the direct application of the solid fuel produced (Antero et al., 2020). There are currently limited publications on the energetic aspects of hydrochar recovered from pulp and paper solid wastes. Lin et al. (2015) examined the effect of HTC temperature (180–300 °C) on the conversion of paper sludge into clean solid fuel at a fixed holding time (30 min), solid load and stirring rate (300 rpm) and produced hydrochar with the highest improvement in calorific value at 210 °C (>8%), lower H/C and O/C ratios, reduced nitrogen and sulphur, in addition to lower ash as a result of the reduction in concentrations of chlorine, sodium and potassium species. Oumabady et al. (2020) optimised the HTC process parameters for producing hydrochar from board mill effluent treatment plants with maximum surface area and pore volume, low H/C and O/C ratios, and low ash-residue from the subsequent co-combustion of the hydrochar fuels and commercial coal, and concluded that 200 °C and 10 h was feasible for to produce hydrochar with 6.8 m^2/g surface area, 0.01 cc/g pore volume, and atomic H/C and O/C ratio of approximately 1.16 and 0.45, respectively. Saha et al. (2019b) investigated the fuel characteristics of hydrochar generated from different paper mill sludge at varying temperatures (180–260 °C) for 30 min and reported hydrochar calorific values ranging from 11.4 ± 0.7 to 31.5 ± 3.7 at maximum temperature, depending on the initial substrate. Unlike temperature, the difference in feedstock quality substantially impacted the combustion performance of the derived hydrochar. Mäkelä et al. (2016) examined the effect of additives (HCl and NaOH) on the HTC treatment of mixed sludge and

found that acidic conditions had a statistically significant effect on the hydrochar energy yield with theoretical energy efficiencies ranging from 97 to 147%. Moreover, higher reaction temperatures enhanced the biological decomposition of the organic matter in the liquid phase, making it sufficiently treatable by conventional biological treatment. The influence of the variation of solid load and residence time at subcritical water temperature on the physicochemical aspects of the hydrochar, energy consumption as well as the optimised process conditions to produce the best-quality hydrochar from paper mill wastes and the subsequent evaluation of the electricity generation potential of hydrochar derived from these streams is yet to be reported. Knowledge of these characteristics is crucial for the HTC process scalability and hydrochar fuel applications in combustion and/or co-combustion at coal-fired plants to generate energy. Within this context, this study aims to adopt a statistical tool known as Response Surface Methodology (RSM) to develop models for predicting the optimal processing condition to achieve maximum hydrochar yield and energy content. This investigation involves the following sub-objectives:

i. To design and build a sustainable novel batch HTC reactor autoclave for experimental purposes according to available technical standards to ensure proper functionality and safe operation of the reactor and sample handling.
ii. To assess the suitability of the HTC technology to upgrade unconventional paper mill sludge into clean solid fuel and optimise the operating conditions to produce high value hydrochar fuel by studying the effect of reaction temperature, residence time, and solid load on the mass yield and calorific value using RSM.
iii. To illustrate the influence of these parameters on the physicochemical characteristics and combustion behaviour of the produced solid fuels to demonstrate their potential for further energetic applications.
iv. To perform an energy balance of hydrochar fuel production from paper sludge by HTC to further evaluate the HTC process energy efficiency and the potential of using heat recovery from the hydrochar fuel.
v. To estimate the electricity generation potential at the optimised HTC reaction conditions for one of South Africa's coal-fired power stations to emphasise the potential for combustible applications.

2. Materials and methods

2.1. Raw material

Raw fibre rejects (RF) from the repulping process, consisting of 21.1% moisture on air-dried basis (wt. %), were collected from Mpact (South Africa). The samples were stored in a polycan container and maintained in a cold room for subsequent examination and experimentation.

2.2. Autoclave reactor design

A laboratory-scale reactor autoclave was designed at the Department of Chemical Engineering, Water Utilisation Division (South Africa), according to mechanical designs for a cylindrical vessel under internal pressure to produce enough hydrochar for analysis from the experiments (Sinnott, 1993). The assembled reactor is illustrated in Fig. 1.

2.3. HTC experiments

For each HTC experimental run, approximately 100 g of the samples consisting of feedstock and deionised water at varying solid loads (8%, 10% and 12%) were stirred manually for 3 min and transferred into the vessel according to previously reported preliminary studies (Assis et al., 2021). The reactor was placed in a preheated oven at $T_{set} - 50°C$, and

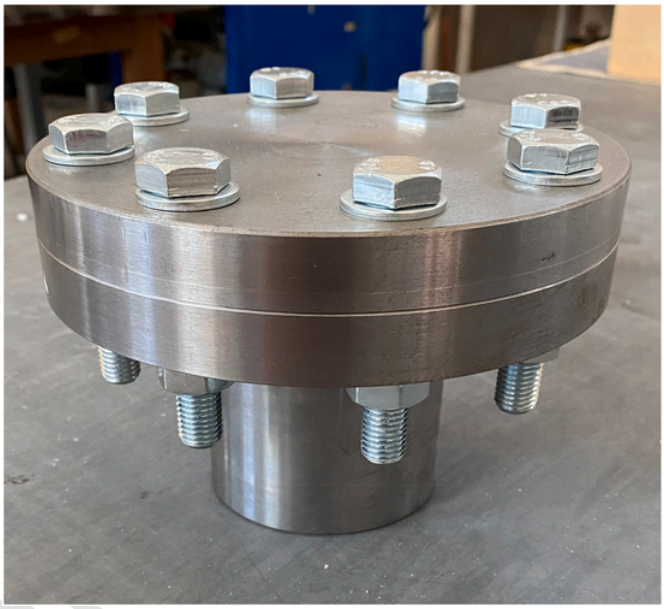

Fig. 1. Visualization of the assembled reactor.

allowed to heat up to the desired carbonisation temperature at a 2.5 °C/min rate. Following carbonisation, the sealed vessel was immersed in flowing water for 10–15 min and cooled to about 21 °C (Nakason et al., 2018). The carbonised material was removed, filtered using a cellulose phosphate-free filter paper with mean 4–12 μm particle size retention (grade MN 615, USA) and subsequently oven-dried at 105 °C for 12 h. For rapid homogenisation and smaller particle size, an electric grinder (Breville Coffee & Spice Grinder) was employed to process the dry samples for 1 min and passed through a 250 μm sieve for all subsequent analyses.

2.4. Experimental design

A Response Surface Methodology (RSM) was adopted to investigate the effects of three independent variables: reaction temperature, residence time, and solid load, including their interactions on hydrochar yield and calorific value (HHV). Due to technical limitations, face-centred Central Composite Design (CCD) was employed. Design Expert ® 11.1.0.1 software (Stat Ease Inc, Minneapolis, MN, USA) was used for the CCD and statistical analysis of variance (ANOVA). The factors were coded at $\alpha = \pm 1$, which requires three levels: 1, 0, and +1.

2.4.1. RSM experimental design for hydrochar yield and calorific value models

For improved prediction quality and model reliability, the CCD experiments included 20 runs: 8 factorial points, 6 axial points and 6 central points. The following equation was used to code the three independent variables:

$$X_i = \frac{x_i - x_0}{\Delta x_i} \quad (1)$$

where $i = 1, 2 \text{ and } 3$. X_i and x_i are the dimensionless and the actual values of the independent variable i, x_0 the actual value of the independent variable i at the central point, and Δx_i the step change of x_i corresponding to a unit variation of value. Table 1 shows the coded and uncoded (actual) levels of the independent variables. Prior to the experiment design, RF samples were carbonised at temperatures of 220 °C, 240 °C and 260 °C for 1 h, 3 h and 5 h. Findings are presented in **Supplementary data**. No major difference was observed in hydrochar yield and calorific values obtained at the maximum reaction conditions (260 °C for t > 3 h) compared to shorter reaction residence times.

Table 1
Independent variables and corresponding levels for the RSM design.

Independent variable	Symbol	Coded levels		
		−1	0	1
Temperature (°C)	X_1	210	230	250
Residence time (h)	X_2	0.50	1.75	3.00
Solid load	X_3	0.08	0.10	0.12

Thus, taking this into consideration, as well as the reactor temperature limitations, the experimental design limit was set to a maximum temperature and time of 250 °C and 3 h, respectively, and minimum reaction conditions of 210 °C and 0.5 h, respectively.

The residence time excluded the time required to achieve the set reaction temperature. All experiments were conducted in random sequence and triplicates. The results were averaged and fitted to a second-order polynomial equation to evaluate the correlation between the response variables and the independent variables as follows:

$$Y = \beta_0 + \beta_1 X_1 + \beta_2 X_2 + \beta_3 X_3 + \beta_{12} X_1 X_2 + \beta_{13} X_1 X_3 + \beta_{23} X_2 X_3 + \beta_{11} \times {}_1{}^2 + \beta_{22} \times {}_2{}^2 + \beta_{33} \times {}_3{}^2 + \varepsilon \quad (2)$$

Where, Y represents the hydrochar yield (H_Y, %) and calorific value (HHV, MJ/kg) response variables, β_0, β_i, β_{ii} and β_{ij} represent a constant, the linear terms, the quadratic terms for one variable and the interaction terms (i = 1, 2 and 3; j = 1, 2 and 3; j = 1,2 and 3), respectively, and ε corresponds to random error.

2.4.2. Statistical analysis

The experimental data were analysed by multiple linear regression using the ANOVA approach to fit the second-order polynomial equation and determine the validity and significance of the developed models. The precision and reliability of the models were further assessed using the regression coefficient determinations R^2, adjusted R^2, predicted R^2, lack of fit, adequate precision and F- value and p-value. The model and terms with p-values less than or equal to 0.05 were defined as statistically significant.

2.4.3. Optimum HTC process conditions

Following the fit model determination, the optimal conditions for hydrochar production were determined by solving the equation derived from the final quadratic model and by evaluating the RSM graphs with responses of lowest values for temperature and residence time, maximum solid load for maximum mass yield and HHV.

2.5. Feedstock and hydrochar characterisation

Proximate analysis, i.e. moisture residual (RM), volatile matter (VM) and ash (A) content of the dried feedstock and hydrochar produced at different HTC process conditions, were conducted in a thermogravimetric analyser (Hitachi STA300 TGA-DTA) based on the ASTM method D7582-15 (ASTM, 2015). The FC was estimated according to equation (3), and the values of VM, FC, and A were adjusted to dry basis (db) using equation (4).

$$FC = 100 - RM - VM - A \quad (3)$$

$$VM,\ FC,\ A\ (db) = VM,\ FC\ or\ A \times \left(\frac{100}{100 - RM}\right) \quad (4)$$

The thermogravimetric tests were carried out using the same equipment. In a crucible, a 10 mg sample was heated to 950 °C at 20 °C/min fixed heating rate and 80 mL/min air flow rate, then maintained isothermally for 10 min. Under the non-isothermal conditions, the mass loss (TG) and associated mass loss rate (DTG) of the samples were continuously recorded.

The elemental carbon (C), hydrogen (H), nitrogen (N) and sulphur (S) composition was evaluated by a Flash 2000 Elemental Analyser (Thermo Fisher Scientific) at the University of Johannesburg (South Africa), according to Cai et al. (2017). The analysis was conducted through the combustion of approximately 2 mg of sample in a controlled atmosphere. The gas products in the form of CO_2, H_2O, N_2 and SO_2, and NO_x (which was later reduced to N_2) were subsequently analysed to determine the CHNS composition. The percentage of oxygen weight (O, %) was calculated using equation (5).

$$O = 100 - C - H - N - S - A \quad (5)$$

A bomb calorimeter (Parr 6200 Oxygen Bomb Calorimeter) was used to quantify the caloric value of the samples in terms of HHV according to the ASTM method D5865-19 (ASTM, 2019). For each analysis, 800–1000 mg sample was placed in a crucible, transferred to the vessel, which was then pressurised with oxygen to 3 MPa and combusted. The resulting energy released (evidenced by the increase in water temperature) was recorded and converted to dry matter basis.

The microstructure of the dried and sieved samples was analysed by scanning electron microscopy (SEM) using an FEG SEM microscrope (Zeiss Gemini 2 Crossbeam 540, Oxford Instruments) at a working distance (WD) between 3.6 and 3.8 mm, with fixed magnifications of 1000 and 18,000 times, and a voltage (EHT) of 5 kV. The samples were prepared following the procedure described by Assis and Chirwa (2021).

2.6. Energy balance

The net energy (Q_{net}) was estimated based on the energy required for the HTC process and the energy released during the combustion of the produced hydrochar fuel. The energy required to heat the reactor and keep it at constant temperature was not factored into the energy input (Q_{in}) calculation. This is because the energy input in this case is a process development perspective that varies with reactor design and operating procedures (Mau et al., 2016). Q_{in} was estimated by adding the energy necessary to heat the dry solids and the water content during HTC, assuming the wet substrate is a non-reactive mixture of water and dry solids, according to equation (6).

$$Q_{in} = m_w(H_{w,\ HTC} - H_{w,25}) + m_s C_{p,s}(T_{HTC} - 25) \quad (6)$$

In equation (6), m_w and m_s represent the water and dry matter mass (kg), respectively; $H_{w,\ HTC}$ and $H_{w,25}$ correspond to the enthalpy of water at the set HTC reaction temperature and 25 °C, respectively; $C_{p,s}$ is the approximate specific capacity of sludge, i.e. 1.05 J/kg K, assuming a dry basis (Stoica et al., 2009); and T_{HTC} represents the HTC reaction temperature. Lastly, the output energy (Q_{out}) resulting from hydrochar fuel combustion was determined according to equation (7).

$$Q_{out} = m_{HC} \times HHV_{HC} \quad (7)$$

where m_{HC} and HHV_{HC} represent the dry weight (kg) and calorific value (MJ/kg) of the hydrochar. The total energy consumed by the system to process the hydrochar was calculated from the sum of the energy consumed for heating the oven from room temperature (assuming 25 °C) to the desired HTC reaction temperature and the energy consumed during the set HTC reaction time. Electricity production per year from the optimised hydrochar was estimated according to the equation below:

$$E_{HC}(GWh) = \frac{\eta \times m_{PPMS} \times HHV_{HC}}{3.6 \times 10^3} \quad (8)$$

where E_{HC} represents the electricity generated from the produced hydrochar, η is the average efficiency of coal-fired power plants in South Africa of 0.352 (Eskom, 2021), m_{PPMS} is the mass of hydrochar produced in tonnes, and HHV_{HC} is the calorific value of the solid fuel in

GJ/tonnes. Lastly, the electricity generated from hydrochar (E_{HC}) was compared to the electricity generated at one of the coal-fired power plants in South Africa (E_C), according to equation (9).

$$\frac{E_{HC}}{E_C} \times 100\ \% \tag{9}$$

3. Results and discussions

3.1. Reactor design

Environmental and sustainability aspects were considered when designing a hydrothermal carbonisation reactor. To have an eco-friendly design that would lead to low environmental impact and consider Health, Safety and Environmental (HSE) aspects, factors such as material selection, energy consumption, waste production, reactor durability and efficiency, reactor disassembly and scaling were considered (La Rosa and Cicala, 2015).

3.1.1. Material selection

The laboratory-scale reactor consists of four major parts: the top cover, gasket, polytetrafluoroethylene lining lid and a seamless vessel with a flat end (Supplementary data, Section A, Figure A 1). DIN EN19 Alloy structural steel was selected to fabricate the cylindrical vessel due to its extreme strength, machinability, cost-effectiveness and availability. The material, also designated as 42CrMo4 contains about 0.37–0.44% carbon (C), 0.15–0.35% silicon (Si), 0.65–1.10% manganese (Mn), up to 0.04% phosphorous (P) and sulphur (S), 0.75–1.20% chromium (Cr) and 0.15–0.25% molybdenum (Mo). These metal constituents improve yield strength and hardenability, prevent brittleness and inhibit grain growth of the material, which results in overall excellent quality high tensile steel grade (Black and Kohser, 2017). These properties increase the durability of the reactor, which is an essential component of design for the environment.

The top cover is equipped with a seamless flange and a lid that can be bolted into the flange, thus facilitating access to the internal part of the reactor. This configuration enables the reactor to be opened easily, filled, and tightly closed. A heat-resistant gasket was considered to ensure a proper sealing system and prevent heat energy loss. A removable polytetrafluoroethylene (PTFE) vessel lining was also incorporated due to its highly non-reactive and non-toxic properties to reduce corrosion and sample contamination.

3.1.2. Stress analysis, reactor size and cost estimations

The health and safety of people during installation, maintenance or use of any technology is essential to ensure that a new machine product has the minimum risk to the users, especially if scalability of the reactor is to be considered (Kielesińska, 2020). Based on the design specification and material stress analyses done to test the reactor, a summary of the limiting factors of the assembled reactor was developed (Table A 1 and Table A 2). The vessel was designed according to the mechanical design for a cylindrical vessel under internal pressure (Sinnott, 1993). The PTFE lining has an inner diameter of 43 mm and an internal height of 86 mm, resulting in a capacity of about 125 mL, thus set as maximum reactor volume capacity. At subcritical water temperature, the self-generating pressure during hydrothermal carbonisation reactions varies between 1 and 3 MPa (Wang et al., 2018). Thus, the reactor autoclave was designed to operate at pressures to accommodate such pressures. In terms of maximal design temperature, not only the temperature of the substrate was considered, but also the highest temperature possible of the material with the lowest thermal stability. In this case, the maximum allowable temperature was set to 260 °C, which is the temperature limit for the PTFE material (McKeen, 2012). All dimensions and cost estimations have also been described (**Subsection A 3**).

3.2. Fitting of the models

In this study, DoE-RSM was used to study the influence of HTC reaction temperature, residence time and solid load on the mass yield and calorific value of hydrochar obtained from recycling paper waste. The experimental and the predicted values of the response variables for hydrochar production are listed in Table 2. Results show a satisfactory agreement between the experimental and predicted values obtained from DoE-RSM Design. The percentage difference between the experimental and the predicted values for hydrochar yield and calorific values ranged between 0.01-7.55% and 0–1.74%, respectively, with an average percentage difference of 2.11% and 1.64%, respectively. Experimental data was used to calculate the coefficients of the second-order polynomial equation, and the regression coefficients are summarised in the subsequent subsections.

3.3. Response surface analysis of hydrochar yield

By applying multiple regression analysis to the experimental data, the hydrochar yield (H_Y) is expressed as a quadratic regression model of HTC reaction temperature (X_1), residence time (X_2) and solid load (X_3), as given in equation (10).

$$\begin{aligned} H_Y(\%) = {} & 78.41 - 12.38X_1 - 16.81X_2 + 1.02X_3 \\ & - 10.36X_1X_2 + 0.0862X_1X_3 + 0.4487X_2X_3 \\ & - 7.08{X_1}^2 + 2.88{X_2}^2 + 1.86{X_3}^2 \end{aligned} \tag{10}$$

Coefficients of the model were evaluated by regression analysis in order to assess the need to exclude non-significant terms from the model. A large regression coefficient and a low *p*-value for a given term in the model suggest a more significant influence on the corresponding response variables. The F-value of 80.17 and *p*-value of less than 0.0001 suggest that the model was highly significant and adequately fits the response data. In terms of lack of fit, there is a 16.27% chance that a lack of fit this large could occur due to noise. Moreover, the value of the determination coefficient (R^2 = 0.9863) indicates the data was adequately represented by the second-order polynomial, and the model explains 98.63% of the variation in hydrochar yield. Thus, only 1.37% of the total variation was not explained by the model.

Table 2
Experimental design for hydrochar production with experimental and predicted values for hydrochar yield and HHV.

Run No.	T (°C)	t (h)	Solid load	Hydrochar Yield (%)		HHV (MJ/kg, db)	
	X_1	X_2	X_3	Experimental	Predicted	Experimental	Predicted
1	230	1.75	0.12	80.57	81.29	17.51	17.76
2	230	0.5	0.10	94.36	98.10	14.99	14.86
3	210	0.5	0.12	95.37	95.38	14.33	14.33
4	250	0.5	0.08	91.97	90.20	15.98	16.00
5	210	3	0.12	82.27	83.39	17.99	17.99
6	250	3	0.08	35.62	34.96	22.46	22.47
7	230	3	0.10	65.62	64.48	19.85	19.92
8	230	1.75	0.10	76.12	78.41	18.11	17.93
9	250	1.75	0.10	54.66	58.95	19.84	20.06
10	210	0.5	0.08	94.80	94.41	14.24	14.43
11	250	0.5	0.12	93.11	91.52	16.19	16.11
12	230	1.75	0.10	77.58	78.41	18.23	17.93
13	230	1.75	0.10	80.51	78.41	17.71	17.93
14	230	1.75	0.10	81.63	78.41	17.81	17.93
15	230	1.75	0.08	77.38	79.25	18.00	17.69
16	250	3	0.12	38.33	38.07	22.86	22.69
17	230	1.75	0.10	79.59	78.41	17.90	17.93
18	230	1.75	0.10	80.23	78.41	17.69	17.93
19	210	3	0.08	79.68	80.63	17.89	17.98
20	210	1.75	0.10	85.41	83.72	17.20	16.92

For the H_Y model, the *p*-values values of the independent variables, reaction temperature (X_1), reaction time (X_2) and the interaction term (X_1X_2), were lower than 0.0001, indicating that the terms were the most significant model variables and had the most considerable influence on the hydrochar yield. Moreover, the quadratic term of the temperature (X_1^2) with a *p*-value of 0.0016 indicated a relatively weaker influence but was significant in the model response. Terms such as the ratio solid load (X_3), the interaction between reaction temperature and solid load (X_1X_3), the quadratic effect of reaction residence time (X_2^2) and solid load (X_3^2) had *p*-values higher than 0.05, which indicated that these terms had no significant effect on the hydrochar yield, i.e. these terms did not significantly explain the model; therefore they are not significant for optimisation of the hydrochar yield. Thus, to further enhance the reliability of the model, a backward model reduction was performed for *p*-values coded at $\alpha = 0.1$ to consider only the significant terms. Therefore, the reduced model for hydrochar yield in terms of the coded equation was given as follows:

$$H_Y(\%) = 78.64 - 12.38X_1 - 16.81X_2 - 10.36X_1X_2 + -6.38{X_1}^2 + 3.57{X_2}^2 \quad (11)$$

The new model has as a higher F-value than the full model ($F = 155.96$; $p < 0.0001$), non-significant Lack of Fit ($F = 2$; $p = 0.2311$), higher adjusted R^2 value (0.9761) and higher adequate precision (43.7416). The reduced ANOVA quadratic regression model for hydrochar yield and (H_Y) is presented in Table 3.

3.4. Response surface analysis of calorific value

By applying multiple regression analysis to the experimental data, the calorific value (HHV) is expressed as a quadratic regression model of HTC reaction temperature (X_1), residence time (X_2) and solid load (X_3), as given by equation (12).

$$\text{HHV (MJ/ kg)} = 17.93 + 1.57\ X_1 + 2.53X_2 + 0.031X_3 + 0.73X_1X_2 + 0.0525X_1X_3 + 0.025X_2X_3 + 0.5623{X_1}^2 - 0.5377{X_2}^2 - 0.2027{X_3}^2 \quad (12)$$

The F-value of 168.28 and *p*-value less than 0.0001 indicate that the model was highly significant and adequately fits the response data. In terms of Lack of Fit, there is a 31.23% probability that a lack of fit of this magnitude could occur due to noise. Moreover, the value of the determination coefficient ($R^2 = 0.9934$) indicates the data was adequately represented by the second-order polynomial, and the model explains 99.34% of the variation in HHV. Thus, only 0.66% of the total variation was not explained by the model.

For the HHV model, the *p*-values values for reaction temperature (X_1), reaction time (X_2) and the interaction term (X_1X_2) were lower than 0.0001, indicating that the terms were the most significant variables and had the largest influence on the calorific value. Furthermore, the quadratic term of the reaction temperature (X_1^2) and residence time (X_2^2) with *p*-values of 0.0039 and 0.0051, respectively, imply a weaker influence but still significant on the model response. Terms such as the solid load (X_3), the interaction between reaction temperature and solid load (X_1X_3), and quadratic effect of solid load (X_3^2) had *p*-values higher than 0.05, which indicates that these terms had no significant effect on the calorific value, i.e. they are not significant for optimisation of the calorific value of the hydrochar. The observed trend on the non-significant influence of the solid load on the hydrochar yield and calorific value is in agreement with Mau et al. (2016). To further improve the reliability of the model, a backward model reduction was performed for *p*-values coded at $\alpha = 0.1$ to consider only the significant terms. Therefore, the reduced model for HHV is given in equation (13).

$$\text{HHV (MJ/ kg)} = 17.90 + 1.57\ X_1 + 2.53X_2 + 0.73X_1X_2 + 0.4862{X_1}^2 - 0.6138{X_2}^2 \quad (13)$$

The new model has as a higher F-value compared to the full model ($F = 341.40$; $p < 0.0001$), higher Lack of Fit (F-value = 1.23; *p*-value = 0.4322), higher adjusted R^2 value (0.9890) and higher adequate precision (63.7181). The reduced ANOVA quadratic regression model for calorific value is presented in Table 4, and the regression coefficients for both reduced models are summarised in Table 5. Results suggest that the data obtained are reliable and the developed models are adequate to make predictions within the design space and optimise HTC process parameters for hydrochar production.

3.5. Effect of process parameters on model responses

3.5.1. Hydrochar yield

Fig. 2 represents the effect of reaction temperature (X_1) and residence time (X_2) on the hydrochar yield at a fixed solid load of 0.10. It is evident from the results that the reaction temperature (X_1) and residence time (X_2) strongly impact hydrochar yield, and the increase in either of the factors results in a drop in hydrochar yield depicted by a

Table 3
Reduced model ANOVA results for hydrochar yield response surface.

Source	SS [a]	df [b]	MS [c]	F-value	p-value
Model	5348.95	5	1069.79	**155.96**	< **0.0001**
X_1	1533.63	1	1533.63	223.59	< 0.0001
X_2	2825.42	1	2825.42	411.92	< 0.0001
X_1X_2	859.26	1	859.26	125.27	< 0.0001
X_1^2	130.31	1	130.31	19.00	0.0007
X_2^2	40.87	1	40.87	5.96	0.0285
Residual	96.03	14	6.86		
Lack of Fit	75.12	9	8.35	2.00	0.2311
Pure Error	20.91	5	4.18		
Cor. Total	5444.98	19			
Model statistics					
Std. Dev.	2.62		R^2	0.9824	
Mean	77.24		Adjusted R^2	0.9761	
C.V. %	3.39		Predicted R^2	0.9577	
			Adeq. Precision	43.7416	

a: sum of squares. b: degree of freedom. c: mean square. p-values < 0.05 indicate model terms are significant.

Table 4
Reduced model ANOVA results for HHV response surface.

Source	SS[a]	df[b]	MS[c]	F-value	p-value
Model	94.23	5	18.85	**341.40**	< **0.0001**
X_1	24.59	1	24.59	445.36	< 0.0001
X_2	64.11	1	64.11	1161.30	< 0.0001
X_1X_2	4.26	1	4.26	77.22	< 0.0001
X_1^2	0.7566	1	0.7566	13.71	0.0024
X_2^2	1.21	1	1.21	21.83	0.0004
Residual	0.7729	14	0.0552		
Lack of Fit	0.5320	9	0.0591	1.23	0.4322
Pure Error	0.2409	5	0.0482		
Cor. Total	95.01	19			
Model statistics					
Std. Dev.	0.2350				
Mean	17.84		R^2	0.9919	
C.V. %	1.32		Adj. R^2	0.9890	
			Pred. R^2	0.9832	
			Adeq. Precision	63.7181	

a: sum of squares. b: degree of freedom. c: mean square. p-values < 0.05 indicate model terms are significant.

Table 5
Regression coefficient values for reduced hydrochar yield and HHV values.

Factor	H_Y		HHV	
	Coefficient estimate	p-value		*p*-value
β_0	78.64		17.90	
Linear effects				
β_1	−12.38	< 0.0001	1.57	< 0.0001
β_2	−16.81	< 0.0001	2.53	< 0.0001
Interaction effects				
β_{12}	−10.36	< 0.0001	0.73	< 0.0001
Quadratic effects				
β_{11}	−6.38	0.0007	0.4862	0.0024
β_{22}	3.57	0.0285	−0.6138	0.0004

p-values less than 0.05 indicate model terms are significant.

response surface with a curved shape. Reaction temperature ($F = 223.59$; $p < 0.0001$) and residence time ($F = 411.92$; $p < 0.0001$) had a highly significant negative linear and interactive effect ($F = 125.57$; $p < 0.0001$) on the hydrochar yield, while reaction temperature alone had a weaker but significant negative quadratic effect on the hydrochar yield ($F = 19$; $p < 0.001$). The hydrochar yield first increased with an increase in reaction temperature and residence time up to a specific point, then decreased with a further increase in reaction temperature and residence time. This finding is consistent with reported literature (Kannan et al., 2017). Within this design space, residence time showed a slightly greater influence on hydrochar yield than reaction temperature. Increasing the residence time from 0.5 h to 3 h at the most severe reaction temperature (250 °C) and fixed solid load of 0.10 resulted in a net 60.64% hydrochar yield decrease, while the decrease in yield as a result of elevating the reaction temperature from 210 °C to 250 °C at the most severe reaction time (3 h) and the solid load of 0.10, led to a net 55.96% hydrochar yield decrease. Thus, the increment of residence time resulted in higher conversion rates. In general, high HTC reaction severity favours the hydrolysis of the polymeric structure of hemicellulose and cellulose into monomers, which consequently undergo a series of reactions involving dehydration, decarboxylation, condensation and polymerisation, resulting in low hydrochar yield (Wang et al., 2018).

The highest hydrochar decrease was observed when the HTC temperature was increased from 230 °C to 250 °C, where a decrease of 46.26% was recorded, compared to a 19.57% decrease when the reaction temperature was increased from 210 °C to 230 °C. Due to its amorphous structure, lower molar mass and less degree of polymerisation compared to cellulose, hemicellulose starts hydrolysing at 180 °C (Wang et al., 2018), whilst cellulose, due to higher carbonisation stability, starts slow degradation at 220 °C and lignin starts to slowly break down at 255 °C (Saha et al., 2019a). Thus, as the temperature approaches 250 °C, both hemicellulose and cellulose almost completely decompose translating into a significant mass loss by the solid phase. These results are consistent with previous studies for sewage waste-derived hydrochar (Spitzer et al., 2018) and hydrochar prepared from combined paper sludge (Lin et al., 2015).

Similarly, the highest hydrochar yield decrease was observed when residence time was increased from 1.75 h to 3 h (41.21%) compared to a 33.79% decrease when residence time was increased from 0.5 to 1.75 h. The minimum hydrochar yield observed was 35.62% obtained at 250 °C for 3 h at a solid load of 0.08, while the maximum hydrochar yield recorded was 95.37% obtained at 210 °C for 0.5 h at a solid load of 0.12.

3.5.2. Calorific value

The calorific value is a vital factor, as it indicates the amount of total energy present in the hydrochar. Fig. 3 depicts the influence of reaction temperature and residence time on the calorific value for a given solid load of 0.10. Similar to hydrochar yield, the reaction temperature (X_1) and residence time (X_2) significantly impacted the calorific value; contrary to the hydrochar yield pattern, increasing the reaction temperature and time resulted in hydrochar with a higher calorific value. The reaction temperature ($F = 445.36$; $p < 0.0001$) and residence time ($F = 1161.30$; $p < 0.0001$) exhibited a highly significant positive linear and interactive effect ($F = 77.22$; $p < 0.0001$) on the calorific value. Moreover, reaction temperature had a weaker but significant positive quadratic effect on the hydrochar yield ($F = 13.71$; $p < 0.01$), while the residence time had a weaker but significant negative quadratic effect on HHV ($F = 21.83$; $p < 0.01$); This implies that the calorific value increased with an increase in reaction temperature and time and then decreased with a further increase in reaction time.

Since the HHV in lignocellulose biomass follows the following trend lignin > cellulose > hemicellulose > extractives > ash (Kambo and Dutta, 2015), higher reaction severity favours an increased rate of devolatilisation of components with lower thermal stability (cellulose and hemicellulose) and increases the content of fractions with higher thermal stability (lignin). As a consequence, hydrochar with a higher calorific value is obtained (Kang et al., 2013).

The maximum HHV recorded was 22.86 MJ/kg, approximately equivalent to the HHV of coal used for commercial utility in South Africa (Makgato and Chirwa, 2017). The maximal HHV observed corresponds to an increase of 49.80% of the HHV of the original feedstock and was obtained at 250 °C, the reaction time of 3 h and the solid load of 0.12. The minimum hydrochar yield recorded was 14.24 MJ/kg obtained at 210 °C for 0.5 h at a solid load of 0.08.

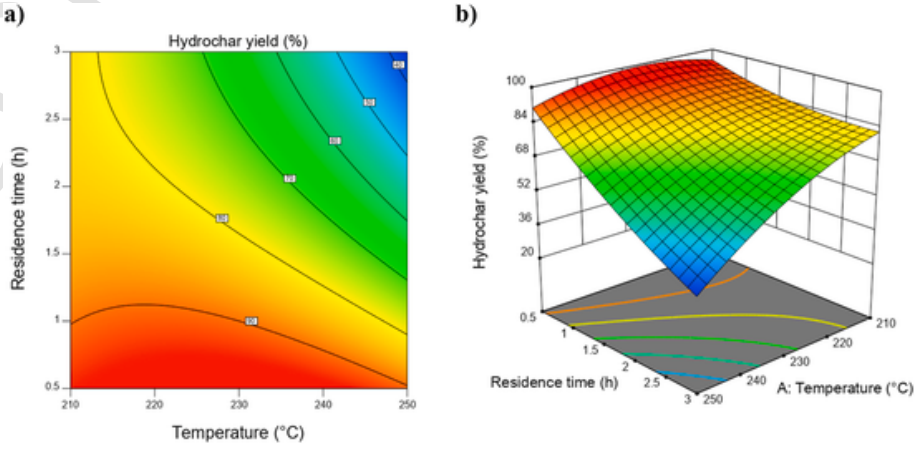

Fig. 2. a) Contour and b) 3D response surface plots showing the effect of temperature and reaction time on the hydrochar yield.

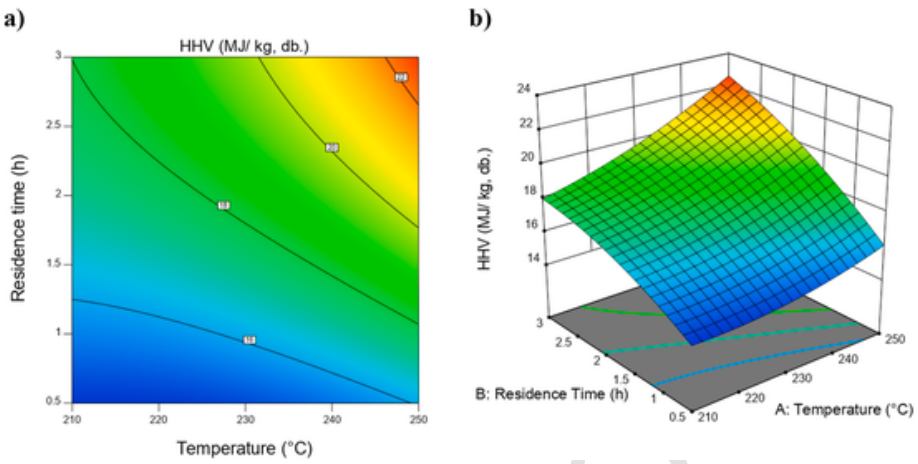

Fig. 3. b) Contour and a) 3D response surface plots showing the effect of temperature and residence time on the calorific value.

3.6. Optimal operating conditions

To obtain optimum conditions, the need for minimum HTC reaction temperature and residence in combination with maximum solid load were considered (i.e. 12 % wt. dry sludge with 88% water) to minimise costs associated with the energy required to heat the water. The goal was to obtain maximal hydrochar yield and calorific value of at least 17 MJ/kg, which falls in the range of the HHV of meta-lignite/sub-bituminous coal calorific values on an ash-free basis (Grammelis et al., 2016). Thus, based on the defined limits under the design space investigated, a maximal solid yield of **74.39%** with a calorific value of **18.50 MJ/kg** was obtainable at the reaction temperature of **231.62 ± 1 °C** and residence time of **1.99 h**, thus considered the optimal HTC operating conditions.

3.7. Hydrochar characteristics

3.7.1. Proximate composition

The proximate composition and the elemental analysis of the raw sludge and hydrochars presented in Table 6 are vital to ensure the efficient application of hydrochar fuels. The initial substrate contains relatively high volatile matter, low fixed carbon, high ash and low fuel ratio. These characteristics, in addition to the high moisture (Assis and Chirwa, 2021), contribute to poor combustion efficiency during heat or power recovery through incineration, and the substantial energy demand for active pre-drying of the sludge has negative environmental impacts mainly due to the emissions of GHG. From the results, it is evident that, in contrast to reaction temperature and residence time, the solid load had little influence on the volatile matter (VM) and fixed carbon (FC) composition. The initial VM and FC were 60.22% and 25.90%, respectively. However, HTC reactions conducted at a residence time of 0.5 h resulted in a gradual increase in volatile matter and a decrease in fixed carbon, which consequently translated into a lower fuel ratio than the original substrate. In contrast, VM had a negative correlation, and FC had a positive correlation when HTC reaction time was ≥1.75 h and with a further increase in reaction severity, leading to a substantial decrease in VM with a simultaneous increase in FC. The maximum VM decrease and FC increment were observed at the highest reaction severity (SF = 6.67, **Supplementary data**), where the VM reduced by 48.75% while the FC increased by approximately 2.14 times compared to the initial substrate. As a result, hydrochars with improved energy densification and enhanced fuel properties were obtained (Table 7). This results from carbonisation mechanisms observed in previous reports for the hydrothermal treatment of cellulose (Saha et al., 2019a), olive mill wastes (Volpe et al., 2018) and lignocellulosic biomass (Hoekman et al., 2011). The increased fuel ratio (characterised by the ratio of fixed carbon to volatile matter content) obtained at higher reaction severity suggests improved combustibility of the hydrochar fuel (Afolabi et al., 2020). The fuel ratio of the produced hydrochar increased from 0.43 to 1.86, with the greatest value recorded at HTC reaction temperature of 250 °C, duration of 3 h and a solid load of 0.08. In comparison to the initial substrate, hydrochar with higher FC and lower VM can be ignited

Table 6
Proximate and elemental analysis of raw sludge at hydrochars at obtained different HTC reaction conditions.

Operating parameters			Proximate composition (db)				Elemental composition (db)				
T (°C)	t (h)	Solid load	VM (%)	FC (%)	Ash (%)	Fuel Ratio	C (%)	H (%)	O[a] (%)	N (%)	S (%)
		Raw sludge	60.22	25.90	13.88	0.43	39.30	5.12	39.44	BD	2.27
210	0.5	0.08	67.81	24.90	7.28	0.37	41.79	5.46	44.56	0.40	0.50
		0.12	69.73	23.92	6.35	0.34	40.88	5.26	46.91	0.21	0.38
	1.75	0.10	64.69	26.08	9.24	0.40	46.10	6.18	37.68	0.32	0.48
	3	0.08	63.82	29.19	6.99	0.46	46.23	5.84	40.63	0.31	BD
		0.12	61.27	30.26	8.47	0.49	47.42	5.93	37.37	0.33	0.49
230	0.5	0.10	70.44	24.41	5.15	0.35	35.62	4.46	54.20	0.21	0.37
	1.75	0.08	60.79	30.36	8.85	0.50	46.40	5.83	38.13	0.32	0.47
		0.10	59.81	31.59	8.60	0.53	46.10	5.76	38.71	0.35	0.49
		0.12	56.85	33.15	10.00	0.58	43.43	5.36	40.86	BD	0.35
	3	0.10	48.22	43.76	8.01	0.91	47.93	5.38	37.82	0.38	0.48
250	0.5	0.08	73.02	22.70	4,28	0.31	41.67	5.93	47.30	0.34	0.48
		0.12	65.62	25.70	8.68	0.39	42.06	5.47	43.39	0.39	BD
	1.75	0.10	39.32	47.47	13.21	1.21	50.25	5.14	30.98	0.42	BD
	3	0.08	29.83	55.40	14.77	1.86	56.27	4.71	23.22	0.51	0.52
		0.12	30.86	52.59	16.55	1.70	57.13	4.97	20,33	0.50	0.53

Table 7
Carbon and energy properties of hydrochars obtained at different HTC reaction conditions.

Operating parameters			Carbon properties			Energy properties		
T (°C)	t (h)	Solid load	C_{char} (%)	C_D	$C_{increase}$ (%)	E_D	$HHV_{improvement}$ (%)	E_Y (%)
210	0.5	0.08	99.88	1.06	6.36	0.93	−6.64	88.51
		0.12	98.29	1.04	4.05	0.94	−6.07	89.58
	1.75	0.10	99.28	1.17	17.34	1.13	12.71	96.27
	3	0.08	92.87	1.18	17.65	1.17	17.23	93.41
		0.12	98.35	1.21	20.68	1.18	17.94	97.03
230	0.5	0.10	84.74	0.91	−9.35	0.98	−1.74	92.72
	1.75	0.08	90.51	1.18	18.09	1.18	17.97	91.28
		0.10	92.12	1.17	17.32	1.17	17.38	93.03
		0.12	89.07	1.11	10.54	1.15	14.79	92.49
	3	0.10	79.30	1.22	21.99	1.30	30.12	85.39
250	0.5	0.08	96.61	1.06	6.05	1.05	4.73	96.32
		0.12	98.74	1.07	7.05	1.06	6.13	98.82
	1.75	0.10	69.26	1.28	27.90	1.30	30.02	71.07
	3	0.08	50.53	1.43	43.23	1.47	35.62	52.43
		0.12	55.22	1.45	45.41	1.50	49.85	57.45

easily at relatively low temperatures and achieve maximum weight loss when combusted (Wang et al., 2018), which consequently translates to enhanced combustion efficiency and lower emissions of pollutants into the environment (Liu et al., 2013).

The energetic application of high-ash hydrochar fuel has negative environmental implications. Therefore, fuels with low ash content are of utmost advantage. In general, the ash composition was relatively lower than the initial substrate. This could be attributed to the dissolution of inorganics into the liquid phase during HTC reaction mechanisms at SF ≤ 6.44. However, the hydrochar obtained at 250 °C and 3 h showed a gradual increase in content from 13.88 to 14.77% and 16.55% at solid loads of 0.08 and 0.12, respectively, due to the retention of inorganics in the solid phase (McGaughy and Reza, 2018). The ash content values obtained in the present study were lower than those reported in hydrochar preparation from paper waste in earlier research. For instance, previous studies have reported ash content of 39.9% (Oumabady et al., 2020), an adjustment from 5.2 ± 0.1% to 50.5 ± 1.5% (Saha et al., 2019b) and from 54.82 ± 1.66% to 66.23 ± 1.78% (Lin et al., 2015). These results suggest the efficiency of HTC in reducing inorganic pollutants under appropriate reaction severities, thereby generating cleaner solid fuel.

3.7.2. Elemental composition

The raw sludge presented low carbon and high oxygen content in the raw sludge making its application as solid fuel environmentally unsustainable. However, the low levels of nitrogen and sulphur results in lower emissions of pollutants in the form of gases. In terms of elemental composition, the solid load had minimal effect on the chemical composition of the hydrochar. Compared to the raw sample, the hydrochars generated at higher reaction severities showed substantial variations in elemental CHONS composition. Previous research has shown similar observations (Saha et al., 2019b). All hydrochars obtained had higher carbon content and, in most cases, lower oxygen fractions. The carbon increased from 39.30% to 57.13% due to carbonisation mechanisms, resulting in a carbon densification factor higher than 1 in all cases except for hydrochar obtained at 230 °C, 0.5 h and a solid load of 0.10 (see Table 7). The range of 1–1.5 in carbon densification factor was in line with previous research on the microcrystalline cellulose-derived hydrochar at 225–275 °C (Lu et al., 2013). Moreover, the values of the carbon retained in the hydrochar ranged from 50.53 to 99.98%. This suggests that after HTC, most of the carbon fraction remained in the solid phase. The substantial reduction in carbon content at the highest reaction severity could be associated with the increased rate of decarboxylation.

The influence of carbon and oxygen fractions on the calorific value of the samples have also been investigated. In terms of carbon content, the results suggest a strong linear correlation (R^2 = 0.8872; p < 0.0001) between the HHV and the carbon content of the initial substrate and the produced hydrochars, as shown in Fig. 4. This trend is consistent with the reported HHV-carbon correlation of hydrochar prepared from coffee solid residues at 180–220 °C (Afolabi et al., 2020) and fish wastes HTC at 150–210 °C (Kannan et al., 2017); this suggests that increased carbon content produces hydrochars with higher calorific values. There was also a strong linear correlation (R2 = 0.8572; p < 0.0001) between the HHV and the oxygen content of the initial substrate and the produced hydrochars, as shown in Fig. 5; this implies that, contrary to carbon content, reducing the oxygen content leads to hydrochar with higher calorific values.

The elemental CHO compositions were used to determine the atomic H/C and O/C ratios, which were then evaluated using the Van Krevelen diagram, as illustrated in Fig. 6, to examine the reaction mechanisms and degree of coalification involved in the HTC treatment of recycling paper fibre sludge. For this analysis, the samples have been labelled as reaction temperature-time-solid load. The atomic H/C and O/C ratios of the hydrochars obtained at 0.5 for h, temperatures of 210 °C and 250 °C, and solid loads of 0.12 and 0.08, respectively, were higher than that of the raw substrate. Apart from this case, the H/C and O/C ratios decreased with an increase in reaction severity.

The ratios of the hydrochars obtained at 0.5 h, temperatures of 210 °C, 230 °C and 250 °C and solid loads of 0.08, 0.10 and 0.12, respectively, moved from the upper left to the lower right, suggesting that

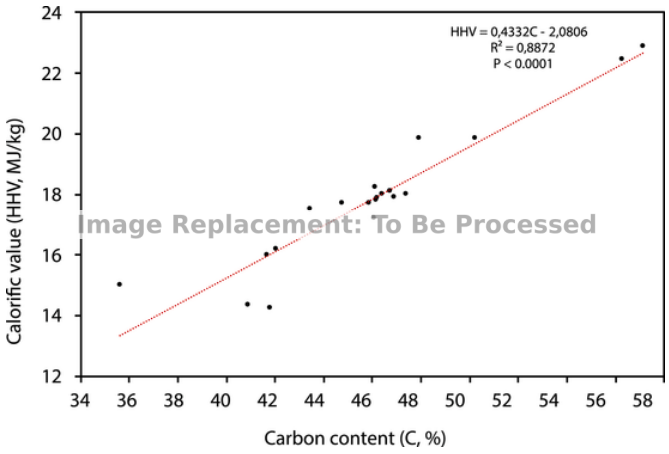

Fig. 4. Correlation between the raw sample and hydrochars carbon content and calorific values.

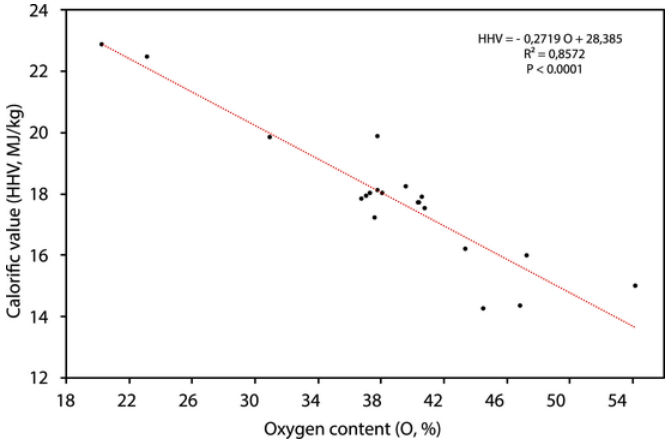

Fig. 5. Correlation between the raw sample and hydrochars oxygen content and calorific values.

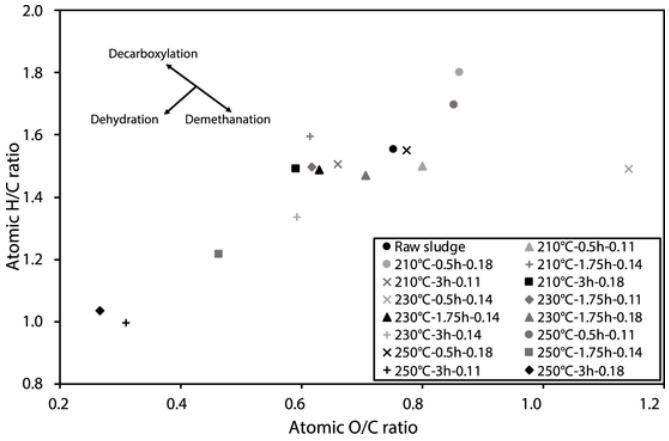

Fig. 6. Van Krevelen diagram of raw sludge and hydrochars obtained at varying HTC operating conditions.

demethanation occurred. The increase in reaction severity intensified the degree of carbonisation for all other samples, as the ratios of the majority of the hydrochars samples moved from the upper right to the lower left and some even moved as far as the upper right, implying that under these operating conditions (T = 210–250 °C and t = 1.75–3 h), the hydrothermal degradation of raw sludge is primarily governed by dehydration and decarboxylation reactions. During dehydration, the hydroxyl groups are eliminated, whereas, in decarboxylation, the long-chain organic components containing carbonyl and carboxyl groups undergo thermal cracking (Funke and Ziegler, 2010), resulting in hydrochar with a higher carbon aromatic structure with enhanced hydrophobicity and thermal stability (He et al., 2013). This is evident by the substantial decrease in ratios, especially at 250 °C, where the H/C and O/C decreased by approximately 35.50% and 64%, respectively. This trend is consistent with reported studies (Berge et al., 2011).

For fuel applications, low H/C and O/C atomic ratios are desired as they reduce smoke, water vapour and energy losses during incineration (Kambo and Dutta, 2014). These characteristics make the hydrochar fuel environmentally friendly due to reduced volatile matter and GHG emissions (Pauline and Joseph, 2020). The quality of the hydrochar produced at more severe carbonisation treatment resembles that of peat/lignite and even sub-bituminous coal (Basu, 2018). These results further suggest the improvement of hydrochar fuel properties as a result of hydrothermal carbonisation. Wang et al. (2020) studied the effect of HTC treatment on sulphur species and reported a decrease in sulphur composition in the solid and liquid phase at higher reaction temperatures, with a subsequent increase of sulphur in the gas phase. The sulphur fraction obtained in this research substantially decreased. Both sulphur (S) and nitrogen (N) composition remained less than 1% and the ash content was mostly lower. Combustion of hydrochar fuels or co-combustion with coals could lead to reduced emissions of precursors, mainly SO_2 and NO_x, into the environment.

3.7.3. Surface morphology of the RF and hydrochars

The microstructural changes in hydrochars formed under various reaction conditions in comparison to the raw substrate are depicted in Fig. 7. The SEM images reveal that the HTC treatment produced hydrochar with distinctive surface morphology compared to the raw substrate. The morphology of the raw sample consisted of long flat fibril structures with smooth surfaces, which varied with the degree of carbonisation reaction. The fibrous structure was preserved in the hydrochars formed at 0.5 h at all reaction temperatures. However, when the reaction duration was 1.75 h, micro-fissures formed in the hydrochar, and the fibres got shorter, rougher and with more uneven surface as the reaction temperature increased. At maximal reaction time (3 h), the hydrochar displayed microstructural fragmentation, formation of agglomerated particles, and porous features. When the HTC temperature was raised to 250 °C, the agglomerated particles increased substantially, and the fibrous structure completely disintegrated. These findings are consistent with hydrochar prepared from paper board sludge (Oumabady et al., 2020) and demonstrate that organic components, namely cellulose and hemicellulose, degraded as a consequence of hydrothermal decomposition during the HTC process (Gai et al., 2016). Furthermore, micro-fissures, fragmentations, and improved porosity properties have a positive influence on the thermal reactivity of the hydrochar fuel during incineration because they facilitate air access and distribution. This property offers an additional advantage for chemical or physical activation (Sevilla and Fuertes, 2016) to produce sustainable porous carbon material for catalysis (Laginhas et al., 2016) or improved adsorbent application for the removal of environmental contaminants, including heavy metals (Sophia A and Lima, 2018) and organic compounds (Zhang et al., 2019), as well as recovery of nutrients such as nitrogen and phosphate from wastewater.

3.7.4. Thermal combustion behaviour

The TG and DTG profiles of the raw sample and derived hydrochars obtained under various HTC treatment conditions are shown in Fig. 8 and Fig. 9. The complete combustion of the samples occurred in four major stages. The peaks at the first stage, which occurred between 50 and 150 °C for all samples, are attributed to residual moisture loss caused by dehydration reactions. At this point, the raw substrate had a maximum peak temperature of around 0.076 °C/min, whereas the hydrochars had a peak temperature ranging from 0.014 to 0.054 °C/min. Fig. 8 shows that the residual moisture reduced following HTC treatment, indicating an improvement in the hydrophobic characteristics of the hydrochar. Following dehydration, the materials exhibited two phases of combustion. The first stage, which occurred between 200 °C and 400 °C, is primarily related to the volatile matter release in the form of cellulose and hemicellulose (Poomsawat and Poomsawat, 2021), which leads to char combustion. The second combustion stage, which took place between 400 °C and 600 °C, is connected with the oxidation of carbonaceous material (char) in the form of lignin and residual volatile matter in the samples. The peaks diminish at the devolatilisation stage and increase at the char combustion phase as the reaction severity increases, demonstrating the breakdown of cellulose and hemicellulose and the accumulation of fixed carbon in the form of lignin (Xiao et al., 2012). The last stage, regarded as the burnout stage, occurred at temperatures higher than 600 °C, and the peaks are attributed to the oxidation of inorganic volatiles, leading to complete combustion. The rate of mass loss was much lower for the hydrochar formed at maximal reaction severity, implying greater thermal stability compared to the raw substrates.

3.8. Energy assessment

The energy balance of the current study is shown in Table 8. The evaluation was conducted with the premise that the reactor had been heated prior to HTC. The results demonstrate that water consumption substantially impacted the quantity of energy (Q_{in}) required for the HTC process, which increased with a decrease in solid load. This was notably true for the carbonisation of sludge at 250 °C with a solid load of 0.08, which required additional 1.05% energy from an external source to heat the system, mainly due to close to 90% energy needed to heat the water. Under this condition, in addition to accounting for factors such as the energy required to heat the system and heat losses, the process becomes energy-inefficient and unsustainable. A similar trend was observed by Mau et al. (2016) for carbonisation at a solid-to-water ratio of 1:10 and 250 °C, which required between 84 and 103% of the energy input from poultry litter-derived hydrochar combustion. Except for this case, the energy demand for HTC ranged from 41.66% to 88.56%, which is considerably high compared to the 17–27% energy

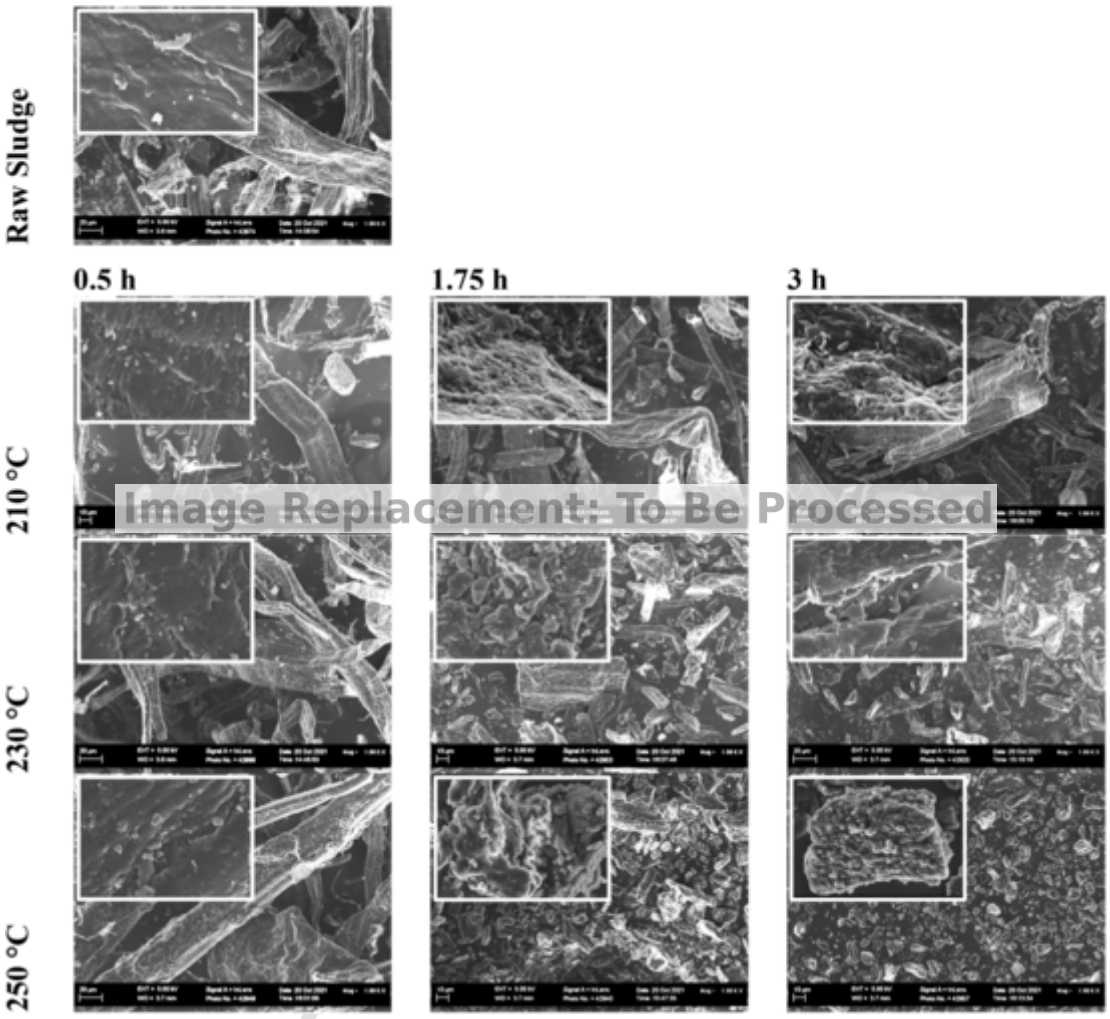

Fig. 7. SEM micrographs of raw sludge and hydrochars obtained at different HTC reaction conditions with magnifications of 1000 and 18000 times.

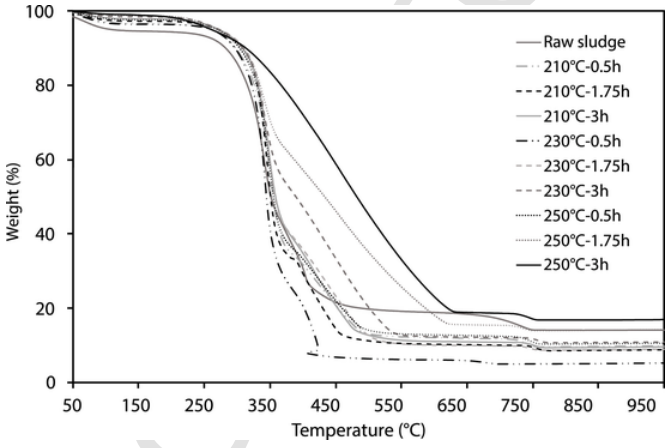

Fig. 8. TG profiles of raw sludge and hydrochars obtained at varying HTC reaction conditions.

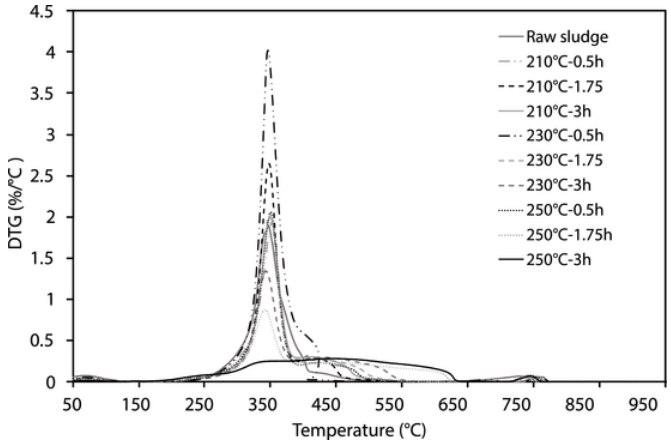

Fig. 9. DTG profiles of raw sludge and hydrochars obtained at varying HTC reaction conditions.

requirement reported by Spitzer et al. (2018) for HTC of human excreta, and the 30.3–37.5% energy demand to treat spent coffee ground wastes at a solid load of 0.1 (Afolabi et al., 2020).

The output energy (Q_{out}) is dependent on the hydrochar yield and the HHV of the produced fuel. Hence, the values were not significantly affected by the solid load fractions but by the variability in reaction temperatures. Therefore, due to the reaction mechanisms discussed in section 3.7, the Q_{out} decreased with increased reaction temperatures. For sustainable fuel application of hydrochar fuel, it is essential to consider the HTC treatment temperature and the quality of the desired fuel. Although higher reaction temperatures generally led to lower energy recovery, the resulting hydrochar offered better quality due to increased energy per unit weight of hydrochar. Up to 58.34% of the energy produced by hydrochar fuel combustion may be recovered as heat

Table 8
Evaluation of energy balance of hydrochar fuel production from RF by HTC, averaged for all residence times.

Solid Load	T(°C)	Q_{water}(kJ)	Q_{sludge}(x10^{-3} kJ)	Total Q_{in}(kJ)	Q_{out}(kJ)	$Q_{recovery}$(%)
0.08	210	71.53	1.51	71.53	107.69	33.57
	230	79.18	1.67	79.19	108.08	26.74
	250	88.82	1.83	88.82	87.87	- 1.08
0.10	210	70.22	1.89	70.23	142.64	50.77
	230	77.61	2.14	77.62	132.79	41.55
	250	86.22	2.28	86.22	104.43	17.44
0.12	210	68.58	2.25	68.59	164.61	58.34
	230	75.45	2.56	75.45	167.60	54.98
	250	83.88	2.73	83.88	137.12	38.83

or power, while the remaining 41.66% of the combustion energy could be utilised to process HTC of paper sludge to produce hydrochar fuel. This finding is slightly higher than the energy recovery of 47.6% reported by Zhao et al. (2014). However, the energy balance accounted for factors such as mechanical dewatering and thermal drying. For a more effective energy recovery, the solid load should be maintained as low as possible while ensuring complete solid dispersion in the reaction medium. Lowering water consumption has additional advantages, such as shorter residence time, early polymerisation, and increased mass yield (Heidari et al., 2019). The process water pH was analysed for all the experiments and varied from 4 to 7. To adhere to the 5 R's of waste management that include reduction, reuse, recycle, recovery and residual management for the industrial-scale application of the HTC, process water under acidic conditions can be reused to catalyse the HTC reactions. Recent literature reported the composition of organic acids (Köchermann et al., 2018), sugars, furans, phenols, cresol and catechol in the liquid phase post-carbonisation treatment (Reza et al., 2014), which could potentially catalyse the hydrothermal decomposition and consequently enhance the fuel properties (Stemann et al., 2013). The process water around neutral pH typically has very low carbon, as indicated in previous studies (Assis et al., 2021). This characteristic will save investments and operating costs associated with organic matter reduction before final discharge.

3.8.1. Energy consumption and environmental impacts

The overall system energy consumption for hydrochar production, the related electricity costs and carbon dioxide equivalent emissions (CO_2e) are presented in Table 9. The total energy consumed ($E_{consumed}$) was estimated taking into account the energy required to heat the oven ($E_{heating}$) at a rate of 2.5 °C/min, the energy consumed for the duration of the HTC reaction (E_{htc}) and the oven wattage of 1500 W at maximum heat. Coal combustion in steam-driven turbine power plants represents about 91% of the electricity generated in South Africa (Makgato and Chirwa, 2017), with average environmental CO_2e emissions of 1.04 kg/kWh (Eskom, 2020). Results from the assessment indicate that higher HTC reaction severity leads to a higher carbon footprint on the environment as a result of the increased energy consumption. Furthermore, the heating stage represents the largest source of pollution. High levels of GHG emissions from coal combustion contribute to global warming and are associated with adverse effects on regional climates (Sher, 1998); thus, increasing the heating rate might substantially reduce environmental emissions. The energy consumption at the optimum operating parameter represents a sustainable option in terms of costs and energy saving, as the carbon emissions are 25% lower than the maximum reaction severities where lower hydrochar yields are achieved.

Table 9
Evaluation of the overall energy consumption, energy cost and carbon dioxide equivalent emissions from hydrochar fuel production from RF by HTC.

T (°C)	$E_{heating}$ (kWh)	$t_{htc\ reaction}$[a] (h)	$E_{htc\ reaction}$ (kWh)	$E_{consume}$[d] (kWh)	E_{cost}[b] ($)	CO_2e[c] (kg)
210	1.85	0.5	0.75	2.60	0.21	2.70
		1.75	2.27	4.12	0.33	4.29
		3	4.50	6.35	0.51	6.60
230	2.06	0.5	0.75	2.81	0.23	2.92
		1.75	2.27	4.33	0.35	4.50
		3	4.50	6.56	0.53	6.82
250	2.25	0.5	0.75	3.00	0.24	3.12
		1.75	2.27	4.52	0.36	4.70
		3	4.50	6.75	0.54	7.02
231.62[c]	2.07	1.99[d]	2.99	5.06	0.41	5.26

[a] : HTC reaction time.
[b] : estimated using the average electricity price in South Africa of $0.08 per kWh for business, as available in September 2021, including all components of electricity, i.e. power, distribution and taxes (Global Petrol Prices, 2021).
[c] : estimated using the electricity grid emission factor of 1.04 kg CO_2e/kWh (Eskom, 2020).
[d] : optimal reaction parameter.

To further assess the energetic potential of hydrochar fuel, the estimation of hydrochar electricity generation at the optimised HTC reaction conditions was compared to electricity generated from coal at one of the coal-fired power stations in South Africa, as presented in Table 10. The Arnot Power Station is located 50 km east of Middleburg and has an efficiency of 35.60% (Eskom, 2021). Over the past three years, the plant produced proximately 9675 GWh (Eskom, 2021), which averages to about 3225 GWh per year. From the optimised results, and considering the substantial amount of the underutilised paper sludge generated on dry weight, the hydrochar fuel recovery could generate over 2 million gigajoules per year, which could sustain about 21% of the energy currently generated from coal at the Arnot power plant, equivalent to ~0.4% of the electricity produced from coal in South Africa in 2020 (Calitz and Wright, 2021). This underlines the potential of paper sludge for an additional renewable energy source, coal replacement or co-combustion while reducing the environmental pollution from the combustion of fossil fuels.

4. Conclusions

This study investigated the effect of HTC process parameters on hydrochar fuel formation from paper sludge. The process was then optimised to maximise the mass yield and calorific value. Upon response surface optimisation, the optimum operating conditions for maximal hydrochar yield (74.39%) and calorific value (18.50 MJ/kg) are achievable at 231 ± 1 °C and 1.99 h. The properties of hydrochars obtained at higher reaction severities exhibited low H/C and O/C ratios and resembled that of lignite, with low sulphur and nitrogen composition and mostly low ash due to reduced inorganic components. The reaction pathways were mainly governed by dehydration and decarboxylation.

Table 10
PPMS hydrochar electricity generation potential for Arnot Coal Power Plant (APP, South Africa).

Parameters	Symbol	Value	Reference
SA amount of paper sludge generated per year (tonnes, db)	m_{PPMS}	500,000	Boshoff et al. (2016)
Optimised hydrochar yield (%)	H_Y	74.39	Present study
Calorific value of hydrochar fuel at optimum condition (GJ/tonnes)	HHV	18.50	Present study
Average efficiency of coal-fired power plants (%)	η	35.20	Eskom (2021)
Proximate electricity production from coal at APP in 2020 (GWh)	E	3225	Eskom (2021)
Electricity generated from coal at APP	E_C	11,610,000	
Electricity generated from hydrochar (GWh)		672.82	
Electricity generated from hydrochar (GJ)	E_{HC}	2,422,152	
Percentage of coal replaceable by hydrochar fuel at APP (%)		20.86	

The hydrochar exhibited cleaner properties compared to the initial substrate, with the potential to be used as a solid fuel for combustion or co-combustion with coal, with reduced emissions of pollutants into the environment. Hydrochar produced under optimal process conditions may generate over 2 million gigajoules of energy per year from the sludge generated annually in South Africa, which is enough to sustain about 0.4% of the total electricity produced from coal in South Africa. The substantial water demand could represent a burden in terms of process sustainability and environmentally friendly disposal. Thus, water recirculation and the potential to catalyse the HTC reactions to increase overall process efficiency should constitute future study to make the process more environmentally friendly for industrial-scale application of HTC.

CRediT authorship contribution statement

Englatina I.N.C. Assis : Methodology, Investigation, Formal analysis, Data curation, Validation, Writing – original draft, Project administration. **Brian Gidudu :** Validation, Writing – review & editing. **EvansM.N. Chirwa :** Conceptualization, Validation, Resources, Writing – review & editing, Supervision, Funding acquisition.

Declaration of competing interest

The authors declare that they have no known competing financial interest or personal relationship that could have appeared to influence the work reported in this paper.

Data availability

Data will be made available on request.

Acknowledgements

Research funding was provided by the Sedibeng Water Chair in Water Utilisation Engineering (Grant No. 4540105923, Rand Water Chair in Water Utilisation and National Research Foundation (NRF), Grant No. IFR200206501999, CSUR210111581519 and EQP210111581520, awarded to Professor Evans M.N. Chirwa of the Water Utilisation and Environmental Engineering Division at the University of Pretoria.

Appendix A. Supplementary data

Supplementary data to this article can be found online at https://doi.org/10.1016/j.jclepro.2022.133775.

References

Afolabi, O.O.D., Sohail, M., Cheng, Y.-L., 2020. Optimisation and characterisation of hydrochar production from spent coffee grounds by hydrothermal carbonisation. Renew. Energy 147, 1380–1391. https://doi.org/10.1016/j.renene.2019.09.098.

Antero, R.V.P., Alves, A.C.F., de Oliveira, S.B., Ojala, S.A., Brum, S.S., 2020. Challenges and alternatives for the adequacy of hydrothermal carbonization of lignocellulosic biomass in cleaner production systems: a review. J. Clean. Prod. 252, 119899. https://doi.org/10.1016/j.jclepro.2019.119899.

Assis, E.I., Chirwa, E.M., 2021. Physicochemical characteristics of different pulp and paper mill waste streams for hydrothermal conversion. Chem. Eng. Trans. 86, 607–612. https://doi.org/10.3303/CET2186102.

Assis, E.I., Chirwa, E.M., Tichapondwa, S.M., 2021. Hydrothermal carbonization of different recycling paper mill waste streams. Chem. Eng. Trans. 88, 43–48. https://doi.org/10.3303/CET2188007.

ASTM, 2015. Standard Test Methods for Proximate Analysis of Coal and Coke by Macro Thermogravimetric Analysis, Method D7582 - 15. PA: ASTM International, West Conshohocken.

ASTM, 2019. Standard Test Method for Gross Calorific Value of Coal and Coke, Method D5865/D5865M-19. ASTM International.

Bajpai, P., 2015. Management of Pulp and Paper Mill Waste. Springer International Publishing. https://doi.org/10.1007/978-3-319-11788-1.

Barbier, J., Charon, N., Dupassieux, N., Loppinet-Serani, A., Mahé, L., Ponthus, J., Courtiade, M., Ducrozet, A., Quoineaud, A.-A., Cansell, F., 2012. Hydrothermal conversion of lignin compounds. A detailed study of fragmentation and condensation reaction pathways. Biomass Bioenergy 46, 479–491. https://doi.org/10.1016/j.biombioe.2012.07.011.

Basu, P., 2018. Chapter 11 - biomass combustion and cofiring. In: Basu, P. (Ed.), Biomass Gasification, Pyrolysis and Torrefaction. third ed., Academic Press, pp. 393–413. https://doi.org/10.1016/B978-0-12-812992-0.00011-X.

Berge, N.D., Ro, K.S., Mao, J., Flora, J.R., Chappell, M.A., Bae, S., 2011. Hydrothermal carbonization of municipal waste streams. Environ. Sci. Technol. 45 (13), 5696–5703. https://doi.org/10.1021/es2004528.

Besse, X., Schuurman, Y., Guilhaume, N., 2015. Hydrothermal conversion of lignin model compound eugenol. Catal. Today 258, 270–275. https://doi.org/10.1016/j.cattod.2014.12.010.

Black, J.T., Kohser, R.A., 2017. DeGarmo's Materials and Processes in Manufacturing, 12 ed. Wiley.

Boshoff, S., Gottumukkala, L.D., van Rensburg, E., Görgens, J., 2016. Paper sludge (PS) to bioethanol: evaluation of virgin and recycle mill sludge for low enzyme, high-solids fermentation. Bioresour. Technol. 203, 103–111. https://doi.org/10.1016/j.biortech.2015.12.028.

Cabrera, M.N., 2017. Pulp mill wastewater: characteristics and treatment. In: Farooq, R., Ah, Z. (Eds.), Biological Wastewater Treatment and Resource Recovery. https://doi.org/10.5772/67537.

Cai, J., He, Y., Yu, X., Banks, S.W., Yang, Y., Zhang, X., Yu, Y., Liu, R., Bridgwater, A.V., 2017. Review of physicochemical properties and analytical characterization of lignocellulosic biomass. Renew. Sustain. Energy Rev. 76, 309–322. https://doi.org/10.1016/j.rser.2017.03.072.

Calitz, J., Wright, J., 2021. Statistics of Utility-Scale Power Generation in South Africa in 2020. Council for Scientific and Industrial Research - Energy Centre.

Chen, C., Liu, G., An, Q., Lin, L., Shang, Y., Wan, C., 2020. From wasted sludge to valuable biochar by low temperature hydrothermal carbonization treatment: insight into the surface characteristics. J. Clean. Prod. 263, 121600. https://doi.org/10.1016/j.jclepro.2020.121600.

Danso-Boateng, E., Holdich, R.G., Martin, S.J., Shama, G., Wheatley, A.D., 2015. Process energetics for the hydrothermal carbonisation of human faecal wastes. Energy Convers. Manag. 105, 1115–1124. https://doi.org/10.1016/j.enconman.2015.08.064.

Department of Energy, 2019. Integrated Resource. Plan (IRP2019). http://www.energy.gov.za/IRP/2019/IRP-2019.pdf (Accessed 12 November 2021).

Eskom, 2020. 2020 Carbon Footprint Report printReport2020.Pdf. https://www.eskom.co.za/wp-content/uploads/2021/09/CarbonFootprintReport2020.pdf (Accessed 10 May 2022).

Eskom, 2021. Coal Fired Power Station. [Online]. https://www.eskom.co.za/eskom-divisions/gx/coal-fired-power-stations (Accessed 12 December 2021).

Fang, J., Zhan, L., O, k.Y.S., Gao, B., 2018. Minireview of potential applications of hydrochar derived from hydrothermal carbonization of biomass. J. Ind. Eng. Chem. 57, 15–21. https://doi.org/10.1016/j.jiec.2017.08.026.

Fuertes, A.B., Arbestain, M.C., Sevilla, M., Maciá-Agulló, J.A., Fiol, S., López, R., Smernik, R.J., Aitkenhead, W.P., Arce, F., Macías, F., 2010. Chemical and structural properties of carbonaceous products obtained by pyrolysis and hydrothermal carbonisation of corn stover. Bioresour. Technol. 48 (7), 618–626. https://doi.org/10.1071/SR10010.

Funke, A., Ziegler, F., 2010. Hydrothermal carbonization of biomass: a summary and discussion of chemical mechanisms for process engineering. Biofuel Bioprod. Biorefin. 4 (2), 160–177. https://doi.org/10.1002/bbb.198.

Gai, C., Guo, Y., Liu, T., Peng, N., Liu, Z., 2016. Hydrogen-rich gas production by steam gasification of hydrochar derived from sewage sludge. Int. J. Hydrogen Energy 41 (5), 3363–3372. https://doi.org/10.1016/j.ijhydene.2015.12.188.

Global Petrol Prices, 2021. South Africa Electricity Prices. https://www.globalpetrolprices.com/South-Africa/electricity_prices.

Gómez, J., Corsi, G., Pino-Cortés, E., Díaz-Robles, L.A., Campos, V., Cubillos, F., 2020. Modeling and simulation of a continuous biomass hydrothermal carbonization process. Chem. Eng. Commun. 207 (6), 751–768. https://doi.org/10.1080/00986445.2019.1621858.

Grammelis, P., Margaritis, N., Karampinis, E., 2016. 2 - solid fuel types for energy generation: coal and fossil carbon-derivative solid fuels. In: Oakey, J. (Ed.), Fuel Flexible Energy Generation. Woodhead Publishing, Boston, pp. 29–58. https://doi.org/10.1016/B978-1-78242-378-2.00002-X.

Güleç, F., Riesco, L.M.G., Williams, O., Kostas, E.T., Samson, A., Lester, E., 2021. Hydrothermal conversion of different lignocellulosic biomass feedstocks – effect of the process conditions on hydrochar structures. Fuel 302, 121166. https://doi.org/10.1016/j.fuel.2021.121166.

He, C., Giannis, A., Wang, J., 2013. Conversion of sewage sludge to clean solid fuel using hydrothermal carbonization: hydrochar fuel characteristics and combustion behavior. Appl. Energy 111, 257–266. https://doi.org/10.1016/j.apenergy.2013.04.084.

Heidari, M., Dutta, A., Acharya, B., Mahmud, S., 2019. A review of the current knowledge and challenges of hydrothermal carbonization for biomass conversion. J. Energy Inst. 92 (6), 1779–1799. https://doi.org/10.1016/j.joei.2018.12.003.

Hoekman, S.K., Broch, A., Robbins, C., 2011. Hydrothermal carbonization (HTC) of lignocellulosic biomass. Energy Fuels 25 (4), 1802–1810. https://doi.org/10.1021/ef101745n.

Holmberg, J.M., Gustavsson, L., 2007. Biomass use in chemical and mechanical pulping with biomass-based energy supply. Resour. Conserv. Recycl. 52 (2), 331–350. https://doi.org/10.1016/j.resconrec.2007.05.002.

Kambo, H.S., Dutta, A., 2014. Strength, storage, and combustion characteristics of densified lignocellulosic biomass produced via torrefaction and hydrothermal carbonization. Appl. Energy 135, 182–191. https://doi.org/10.1016/j.apenergy.2014.08.094.

Kambo, H.S., Dutta, A., 2015. A comparative review of biochar and hydrochar in terms of

production, physico-chemical properties and applications. Renew. Sustain. Energy Rev. 45, 359–378. https://doi.org/10.1016/j.rser.2015.01.050.
Kang, S., Li, X., Fan, J., Chang, J., 2012. Characterization of hydrochars produced by hydrothermal carbonization of lignin, cellulose, d-xylose, and wood meal. Ind. Eng. Chem. Res. 51 (26), 9023–9031. https://doi.org/10.1021/ie300565d.
Kang, S., Li, X., Fan, J., Chang, J., 2013. Hydrothermal conversion of lignin: a review. Renew. Sustain. Energy Rev. 27, 546–558. https://doi.org/10.1016/j.rser.2013.07.013.
Kannan, S., Gariepy, Y., Raghavan, G.S.V., 2017. Optimization and characterization of hydrochar produced from microwave hydrothermal carbonization of fish waste. Waste Manage. (Tucson, Ariz.) 65, 159–168. https://doi.org/10.1016/j.wasman.2017.04.016.
Kaur, R., Tyagi, R.D., Zhang, X., 2020. Review on pulp and paper activated sludge pretreatment, inhibitory effects and detoxification strategies for biovalorization. Environ. Res. 182, 109094. https://doi.org/10.1016/j.envres.2019.109094.
Kielesińska, A., 2020. Safety of imported machines-selected issues in the context of Polish (UE) regulation. System Safety: Human-Technical Facility-Environment 2 (1).
Knez, Ž., Markočič, E., Hrnčič, M.K., Ravber, M., Škerget, M., 2015. High pressure water reforming of biomass for energy and chemicals: a short review. J. Supercrit. Fluids 96, 46–52. https://doi.org/10.1016/j.supflu.2014.06.008.
Köchermann, J., Görsch, K., Wirth, B., Mühlenberg, J., Klemm, M., 2018. Hydrothermal carbonization: temperature influence on hydrochar and aqueous phase composition during process water recirculation. J. Environ. Chem. Eng. 6 (4), 5481–5487. https://doi.org/10.1016/j.jece.2018.07.053.
Kruse, A., Funke, A., Titirici, M., 2013. Hydrothermal conversion of biomass to fuels and energetic materials. Curr. Opin. Chem. Biol. 17 (3), 515–521. https://doi.org/10.1016/j.cbpa.2013.05.004.
La Rosa, A.D., Cicala, G., 2015. 14 - LCA of fibre-reinforced composites. In: Muthu, S.S. (Ed.), Handbook of Life Cycle Assessment (LCA) of Textiles and Clothing. Woodhead Publishing, pp. 301–323. https://doi.org/10.1016/B978-0-08-100169-1.00014-9.
Laginhas, C., Nabais, J.M.V., Titirici, M.M., 2016. Activated carbons with high nitrogen content by a combination of hydrothermal carbonization with activation. Microporous Mesoporous Mater. 226, 125–132. https://doi.org/10.1016/j.micromeso.2015.12.047.
Libra, J.A., Ro, K.S., Kammann, C., Funke, A., Berge, N.D., Neubauer, Y., Titirici, M.-M., Fühner, C., Bens, O., Kern, J., Emmerich, K.-H., 2011. Hydrothermal carbonization of biomass residuals: a comparative review of the chemistry, processes and applications of wet and dry pyrolysis. Biofuels 2 (1), 71–106. https://doi.org/10.4155/bfs.10.81.
Lin, Y., Ma, X., Peng, X., Hu, S., Yu, Z., Fang, S., 2015. Effect of hydrothermal carbonization temperature on combustion behavior of hydrochar fuel from paper sludge. Appl. Therm. Eng. 91, 574–582. https://doi.org/10.1016/j.applthermaleng.2015.08.064.
Liu, Z., Quek, A., Kent Hoekman, S., Balasubramanian, R., 2013. Production of solid biochar fuel from waste biomass by hydrothermal carbonization. Fuel 103, 943–949. https://doi.org/10.1016/j.fuel.2012.07.069.
Lu, X., Pellechia, P.J., Flora, J.R.V., Berge, N.D., 2013. Influence of reaction time and temperature on product formation and characteristics associated with the hydrothermal carbonization of cellulose. Bioresour. Technol. 138, 180–190. https://doi.org/10.1016/j.biortech.2013.03.163.
Mäkelä, M., Benavente, V., Fullana, A., 2016. Hydrothermal carbonization of industrial mixed sludge from a pulp and paper mill. Bioresour. Technol. 200, 444–450. https://doi.org/10.1016/j.biortech.2015.10.062.
Makgato, S.S., Chirwa, E.M., 2017. Waterberg coal characteristics and SO2 minimum emissions standards in South African power plants. J. Environ. Manag. 201, 294–302. https://doi.org/10.1016/j.jenvman.2017.06.049.
Mau, V., Quance, J., Posmanik, R., Gross, A., 2016. Phases' characteristics of poultry litter hydrothermal carbonization under a range of process parameters. Bioresour. Technol. 219, 632–642. https://doi.org/10.1016/j.biortech.2016.08.027.
McGaughy, K., Reza, M.T., 2018. Recovery of macro and micro-nutrients by hydrothermal carbonization of septage. J. Agric. Food Chem. 66 (8), 1854–1862. https://doi.org/10.1021/acs.jafc.7b05667.
McKeen, L.W., 2012. 11 - fluoropolymers. In: McKeen, L.W. (Ed.), Film Properties of Plastics and Elastomers. William Andrew Publishing, Boston, pp. 255–313. https://doi.org/10.1016/B978-1-4557-2551-9.00011-6.
Nakason, K., Panyapinyopol, B., Kanokkantapong, V., Viriya-empikul, N., Kraithong, W., Pavasant, P., 2018. Characteristics of hydrochar and liquid fraction from hydrothermal carbonization of cassava rhizome. J. Energy Inst. 91 (2), 184–193. https://doi.org/10.1016/j.joei.2017.01.002.
Oumabady, S., S, P.S., Kamaludeen, S.P.B., Ramasamy, M., Kalaiselvi, P., Parameswari, E., 2020. Preparation and characterization of optimized hydrochar from paper board mill sludge. Sci. Rep. 10 (1), 773. https://doi.org/10.1038/s41598-019-57163-7.
Paper Manufactory Association of South Africa, 2015. Summary Findings on 2015 Production, Import and Export Statistics. https://www.thepaperstory.co.za/wp-content/uploads/2017/05/PAMSA-2015-stats-report-FINAL.pdf (Accessed 25 May 2020).
Pauline, A.L., Joseph, K., 2020. Hydrothermal carbonization of organic wastes to carbonaceous solid fuel – a review of mechanisms and process parameters. Fuel 279, 118472. https://doi.org/10.1016/j.fuel.2020.118472.
Penninger, J.M.L., Kersten, R.J.A., Baur, H.C.L., 1999. Reactions of diphenylether in supercritical water — mechanism and kinetics. J. Supercrit. Fluids 16 (2), 119–132. https://doi.org/10.1016/S0896-8446(99)00024-8.
Poomsawat, S., Poomsawat, W., 2021. Analysis of hydrochar fuel characterization and combustion behavior derived from aquatic biomass via hydrothermal carbonization process. Case Stud. Therm. Eng. 27, 101255. https://doi.org/10.1016/j.csite.2021.101255.
Reza, M.T., Wirth, B., Lüder, U., Werner, M., 2014. Behavior of selected hydrolyzed and dehydrated products during hydrothermal carbonization of biomass. Bioresour. Technol. 169, 352–361. https://doi.org/10.1016/j.biortech.2014.07.010.
Saha, N., Saba, A., Reza, M.T., 2019a. Effect of hydrothermal carbonization temperature on pH, dissociation constants, and acidic functional groups on hydrochar from cellulose and wood. J. Anal. Appl. Pyrolysis 137, 138–145. https://doi.org/10.1016/j.jaap.2018.11.018.
Saha, N., Saba, A., Saha, P., McGaughy, K., Franqui-Villanueva, D., Orts, W., Hart-Cooper, W., Reza, M., 2019b. Hydrothermal carbonization of various paper mill sludges: an observation of solid fuel properties. Energies 12 (5), 858. https://doi.org/10.3390/en12050858.
Sevilla, M., Fuertes, A.B., 2016. A green approach to high-performance supercapacitor electrodes: the chemical activation of hydrochar with potassium bicarbonate. ChemSusChem 9 (14), 1880–1888. https://doi.org/10.1002/cssc.201600426.
Sher, E., 1998. Environmental aspects of air pollution. In: ESher, E. (Ed.), Handbook of Air Pollution. Academic Press, Boston, pp. 27–41.
Sinnott, R.K., 1993. Chapter 13 - mechanical design of process equipment. In: Sinnott, R.K. (Ed.), Coulson and Richardson's Chemical Engineering. second ed., Pergamon, Amsterdam, pp. 703–796. https://doi.org/10.1016/B978-0-08-041865-0.50021-0.
Smith, A.M., Singh, S., Ross, A.B., 2016. Fate of inorganic material during hydrothermal carbonisation of biomass: influence of feedstock on combustion behaviour of hydrochar. Fuel 169, 135–145. https://doi.org/10.1016/j.fuel.2015.12.006.
Sophia A, C., Lima, E.C., 2018. Removal of emerging contaminants from the environment by adsorption. Ecotoxicol. Environ. Saf. 150, 1–17. https://doi.org/10.1016/j.ecoenv.2017.12.026.
Spitzer, R.Y., Mau, V., Gross, A., 2018. Using hydrothermal carbonization for sustainable treatment and reuse of human excreta. J. Clean. Prod. 205, 955–963. https://doi.org/10.1016/j.jclepro.2018.09.126.
Srivastava, R.K., Shetti, N.P., Reddy, K.R., Kwon, E.E., Nadagouda, M.N., Aminabhavi, T.M., 2021. Biomass utilization and production of biofuels from carbon neutral materials. Environ. Pollut. 276, 116731. https://doi.org/10.1016/j.envpol.2021.116731.
Stemann, J., Putschew, A., Ziegler, F., 2013. Hydrothermal carbonization: process water characterization and effects of water recirculation. Bioresour. Technol. 143, 139–146. https://doi.org/10.1016/j.biortech.2013.05.098.
Stoica, A., Sandberg, M., Holby, O., 2009. Energy use and recovery strategies within wastewater treatment and sludge handling at pulp and paper mills. Bioresour. Technol. 100 (14), 3497–3505. https://doi.org/10.1016/j.biortech.2009.02.041.
Titirici, M.-M., Thomas, A., Antonietti, M., 2007. Back in the black: hydrothermal carbonization of plant material as an efficient chemical process to treat the CO2 problem? New J. Chem. 31 (6), 787–789. https://doi.org/10.1039/B616045J.
Van der Stelt, C, M.J., Gerhauser, H., Kiel, J.H.A., Ptasinski, K.J., 2011. Biomass upgrading by torrefaction for the production of biofuels: a review. Biomass Bioenergy 35 (9), 3748–3762. https://doi.org/10.1016/j.biombioe.2011.06.023.
Volpe, M., Wüst, D., Merzari, F., Lucian, M., Andreottola, G., Kruse, A., Fiori, L., 2018. One stage olive mill waste streams valorisation via hydrothermal carbonisation. Waste Manage. (Tucson, Ariz.) 80, 224–234. https://doi.org/10.1016/j.wasman.2018.09.021.
Wahyudiono, Kanetake, T., Sasaki, M., Goto, M., 2007. Decomposition of a lignin model compound under hydrothermal conditions. Chem. Eng. Technol. 30 (8), 1113–1122. https://doi.org/10.1002/ceat.200700066.
Wahyudiono, Sasaki, M., Goto, M., 2009. Conversion of biomass model compound under hydrothermal conditions using batch reactor. Fuel 88 (9), 1656–1664. https://doi.org/10.1016/j.fuel.2009.02.028.
Wang, T., Zhai, Y., Zhu, Y., Li, C., Zeng, G., 2018. A review of the hydrothermal carbonization of biomass waste for hydrochar formation: process conditions, fundamentals, and physicochemical properties. Renew. Sustain. Energy Rev. 90, 223–247. https://doi.org/10.1016/j.rser.2018.03.071.
Wang, Z., Zhai, Y., Wang, T., Peng, C., Li, S., Wang, B., Liu, X., Li, C., 2020. Effect of temperature on the sulfur fate during hydrothermal carbonization of sewage sludge. Environ. Pollut. 260, 114067. https://doi.org/10.1016/j.envpol.2020.114067.
Xiao, L.-P., Shi, Z.-J., Xu, F., Sun, R.-C., 2012. Hydrothermal carbonization of lignocellulosic biomass. Bioresour. Technol. 118, 619–623. https://doi.org/10.1016/j.biortech.2012.05.060.
Yay, A.S.E., Birinci, B., Açıkalın, S., Yay, K., 2021. Hydrothermal carbonization of olive pomace and determining the environmental impacts of post-process products. J. Clean. Prod. 315, 128087. https://doi.org/10.1016/j.jclepro.2021.128087.
Zhang, X., Gao, B., Fang, J., Zou, W., Dong, L., Cao, C., Zhang, J., Li, Y., Wang, H., 2019. Chemically activated hydrochar as an effective adsorbent for volatile organic compounds (VOCs). Chemosphere 218, 680–686. https://doi.org/10.1016/j.chemosphere.2018.11.144.
Zhao, P., Shen, Y., Ge, S., Yoshikawa, K., 2014. Energy recycling from sewage sludge by producing solid biofuel with hydrothermal carbonization. Energy Convers. Manag. 78, 815–821. https://doi.org/10.1016/j.enconman.2013.11.026.